Camera Model Identification based on the Heteroscedastic Noise Model

Thanh Hai Thai *Student Member, IEEE,*, Rémi Cogranne *Member, IEEE,*, Florent Retraint

***Abstract*—The goal of this paper is to design a statistical test for the camera model identification problem. The approach is based on the heteroscedastic noise model which describes more accurately a natural raw image. This model is characterized by only two parameters which are considered as unique fingerprint to identify camera models. The camera model identification problem is cast in the framework of hypothesis testing theory. In an ideal context where all model parameters are perfectly known, the Likelihood Ratio Test (LRT) is presented and its performances are theoretically established. For a practical use, two Generalized Likelihood Ratio Tests (GLRT) are designed to deal with unknown model parameters so that they can meet a prescribed false alarm probability while ensuring a high detection performance. Numerical results on simulated images and real natural raw images highlight the relevance of the proposed approach.**

***Index Terms*—Hypothesis Testing, Digital Forensics, Camera Model Identification, Natural Image Model, Nuisance Parameters.**

I. Introduction

DIGITAL forensics has received a great attention from law enforcement agencies and academic researchers in the past decades. Because of dramatic advancement in computing and network technologies, the accessibility and transmission of digital images have been increased remarkably. These technologies have been misused by criminals with unlawful or unethical activities. Consequently, the reliability and trustworthiness of digital images have been questioned when used as evidence in legal and security domains. Reliable forensic methods are urgently needed by law enforcement agencies to deal with criminal and malicious purposes.

A. State of the Art

Digital image forensics concerns two key problems: image origin identification and image forgery detection (see [1]–[3] and the references therein for general surveys). The image origin identification aims to verify whether a given digital image was acquired by a specific device or a certain camera model. The image forgery detection aims to detect any act of manipulation such as splicing, removal or adding in an image. There are two approaches to address these problems. Digital watermarking is regarded as an active approach. It has some limitations [3] because the embedding mechanism must be available and the credibility of information embedded in the image remains questionable. Passive forensics has been increasingly studied in the past decade since no watermark or prior information of the image including the availability of original image is required in its operation mechanism. Passive forensics methods rely on camera fingerprints left in the given image to identify its origin and to verify its authenticity. These fingerprints are extracted by investigating the image acquisition pipeline; see [4]–[6] for an overview of the structure and processing stages of a typical digital camera.

Passive forensic methods proposed for the image origin identification problem can be divided into two following fundamental categories:

1) Methods in the first category work on the assumption that there are differences in image processing techniques and component technologies among device models. Lens aberration [7], Color Filter Array (CFA) interpolation and demosaicing algorithms [8]–[12], JPEG compression [13] are considered as influential factors for camera model identification while white balancing algorithms [14] are used for source device identification. Based on these factors, a forensic feature set is provided and used in the machine learning algorithm. The main challenge is that the image processing techniques remain identical or similar, and the components produced by a few manufacturers are shared among camera models. Moreover, as in all application of machine learning, it is difficult to select an accurate feature set. Besides, the analytic establishment of detection performance remains an open problem [15].
2) Methods in the second category aim to identify unique characteristics or fingerprints of the acquisition device. Sensor Pattern Noise (SPN) is caused by imperfections during the manufacturing process and non-uniformity of photo-electronic conversion due to inhomogeneity of sil-

Thanh Hai Thai, Rmi Cogranne and Florent Retraint are with the ICD - LM2S, Universit de Technologie de Troyes (UTT), UMR STMR - CNRS.

Correspondance should be addressed to thanh_hai.thai@utt.fr, to remi.cogranne@utt.fr or to florent.retraint@utt.fr

icon wafers. This is a unique fingerprint which the methods are mainly based on to identify the source device. The reader is referred to [16] for the first version of this work and [17]–[21] for the enhanced version. Moreover, the Photo-Response Non-Uniformity noise (PRNU) was also used in [22] for camera model identification based on the assumption that the fingerprint obtained from images in the TIFF or JPEG format contains traces of post-acquisition processes (e.g. demosaicing) that carry information about the camera model. It is necessary to note that the two main components of the SPN are the Fixed Pattern Noise (FPN) and the PRNU. The FPN, which was used in [23] for the device identification, can be compensated by subtracting a dark frame from the output image. Therefore, the FPN is not a robust fingerprint and no longer used in later works. The PRNU is directly exploited in some works [17], [18], [21]. The ability to reliably extract this noise from the given image is the main challenge in this category. Another challenge is the forgery of the image origin due to counter-forensic activities [24]. However, the existing methods have been designed with a very limited exploitation of hypothesis testing theory and statistical image models. Therefore, their performance remains analytically unestablished.

B. Main Contributions of the Paper

In an operational context, the design of an accurate detector might not be sufficient. Such context requires a test with analytically predictable results guaranteeing a prescribed false alarm rate. This paper aims to design such a statistical test based on the heteroscedastic noise model for the camera model identification. The approach involves the theory of statistical hypothesis testing [25]. Our previous work [26] has designed a Generalized Likelihood Ratio Test (GLRT) to deal with unknown image parameters assuming that the camera parameters are perfectly known. The previous work is extended in this paper to deal with unknown camera parameters in a practical context. The main contributions are the following :

- Far from the conventional Additive White Gaussian Noise (AWGN) model widely used in image processing, the proposed approach is based on the heteroscedastic noise model which describes more accurately natural images [27]–[29]. By physically modeling the image processing pipeline, the model consists of a Poissonian part that addresses the photon shot noise and dark current and a Gaussian part for the remaining stationary disturbances, e.g. read-out noise. The heteroscedastic property gives the noise variance as a linear function of pixel's mathematical expectation. The heteroscedastic noise model is characterized by two camera parameters that can be reliably extracted from a given image and exploited as unique fingerprint to identify camera models.
- The above parametric image model allows to design an optimal detector that is given by the Likelihood Ratio Test (LRT) in an ideal context where all model parameters are known. This optimal detector serves as an upper-bound of any statistical test for the camera model identification problem.

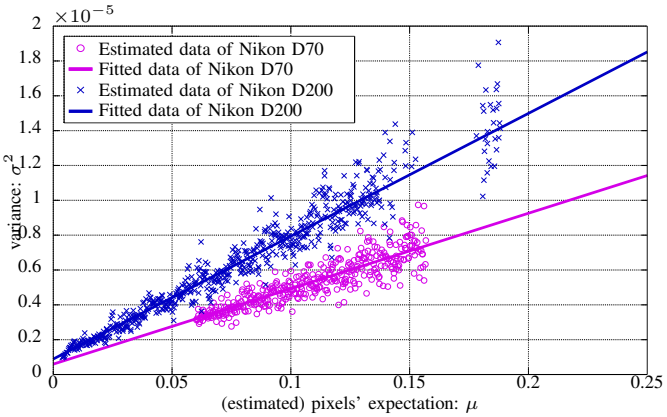

Fig. 1: Scatter-plot of pixels' expectation and variance from a natural raw image [30].

- The paper proposes two Generalized Likelihood Ratio Tests (GLRT) to be adapted for a practical context. The first GLRT is designed to deal with unknown image parameters when assuming that camera parameters are known and the second one for all unknown model parameters. The statistical performance of these GLRTs is analytically established. Moreover, the proposed tests allow the guaranteeing of a prescribed false-alarm rate and the setting of decision threshold independently of the image content, which is crucial for an operation context.

C. Organization of the Paper

The paper is organized as follows. Section II describes the heteroscedastic noise model and presents camera fingerprints to be exploited in this paper. Section III details the methodology for an estimation of camera fingerprints. Section IV states the camera model identification problem in the framework of hypothesis testing theory and studies an optimal detector assuming that all model parameters are known. Section V designs a GLRT to address the difficulty of unknown image parameters. Section VI addresses the context where the image parameters and the camera parameters are all unknown. Section VII presents numerical results of two proposed GLRTs on simulated and real natural raw images. Section VIII discusses about strengths and limitations of the proposed approach. Finally, Section IX concludes the paper.

II. Camera Fingerprint

A. Heteroscedastic Noise Model

This paper deals with natural images which are acquired by a digital imaging sensor. Let us assume that a natural image is a vector $\mathbf{Z} = \{z_i\}_{i \in \mathcal{I}}$ of N pixels where $\mathcal{I} = \{1, \ldots, N\}$ is the index set of pixels. By investigating the image acquisition process, a physical model of natural raw images is given in [29]. The photo-electron conversion essentially consists in a counting process which can be modeled as a Poisson process. The number of collected electrons, denoted Ne_i, is the sum of the electrons generated by the incident photons Np_i and the dark electrons Nt_i generated by thermal noise. Accordingly,

the number of collected electrons Ne_i is given by

$$Ne_i \sim \mathcal{P}(\eta_i Np_i + Nt_i) \tag{1}$$

where $\mathcal{P}(\cdot)$ represents the Poisson distribution and η_i is a conversion factor representing filter transmittance and quantum efficiency. It is assumed that the photo-sensitivity and the thermal noise are constant for every pixel. For the sake of clarity, the index i is therefore omitted from η and Nt. The number of collected electrons is then transferred to a read-out unit. During the read-out process, the recorded signal is corrupted by different sources of electronic noise which all can be modeled as a zero-mean Gaussian random variable ξ_i with variance ω^2, (see details in [29]). This Gaussian noise is stationary and independent of the signal. The noisy raw pixel intensity z_i is finally given by:

$$z_i = g \cdot (Ne_i + \xi_i) \tag{2}$$

where g is the analog gain controlled by the choice of the ISO sensitivity setting. It is important to note that raw pixels are statistically independent [28], [29], i.e. the noise corrupting each pixel is independent of those of neighbor pixels. For the sake of simplification, the normal approximation of the Poisson distribution may be exploited because of a large number of counted electrons. It follows that

$$z_i \sim \mathcal{N}(\mu_i, a\mu_i + b) \tag{3}$$

where $\mathcal{N}(\cdot)$ represents the Gaussian distribution, $\mu_i = g \cdot (\eta Np_i + Nt)$ is the expected value of raw pixel z_i and the parameters (a, b) are given by the following relation

$$a = g \quad \text{and} \quad b = g^2\omega^2. \tag{4}$$

In this paper it is assumed that the phenomenon of clipping is absent from a natural raw image, i.e. the probability that one observation z_i exceeds over the boundary 0 or $2^B - 1$ is negligible (see details about the phenomenon of clipping in [27], [28]. The statistical distribution of raw pixel and the heteroscedastic relation become non-linear, which cause a difficulty of designing the statistical test. This difficulty lies outside the scope of the paper. Accordingly, the phenomenon of clipping will not be studied in this paper.

B. Camera Parameter Property

In some digital imaging sensors, the collected electrons Ne_i may be added by a base pedestal parameter p_0 to constitute an offset-from-zero of the output pixel [28]

$$z_i = g \cdot \Big[p_0 + \mathcal{P}(\eta_i Np_i + Nt_i - p_0) + \mathcal{N}(0, \omega^2)\Big]. \tag{5}$$

Hence, the parameters (a, b) are now given by

$$a = g \quad \text{and} \quad b = g^2\omega^2 - g^2 p_0. \tag{6}$$

Therefore, the parameter b can be negative when $p_0 > \omega^2$, see Fig. 2.

From the relation (4) and (6), the camera parameters (a, b) mainly depend on the ISO sensitivity via the analog gain g. If the digital imaging sensor does not add a pedestal parameter p_0, the parameter a is proportional to ISO sensitivity while the parameter b is proportional to its square. It should be noted that other camera settings such as integration time, shutter speed or focal length can also affect the parameters (a, b). However, those effects are very small compared with the effect of ISO sensitivity. Therefore, this paper addresses the effect of ISO sensitivity and allows a variation of other camera settings.

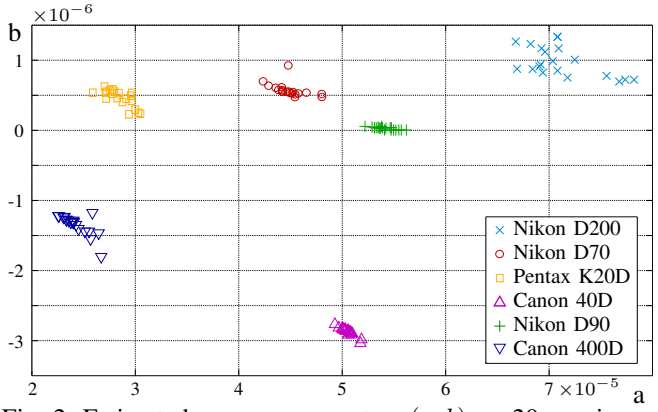

Fig. 2: Estimated camera parameters (a, b) on 20 raw images of different camera model with ISO 200.

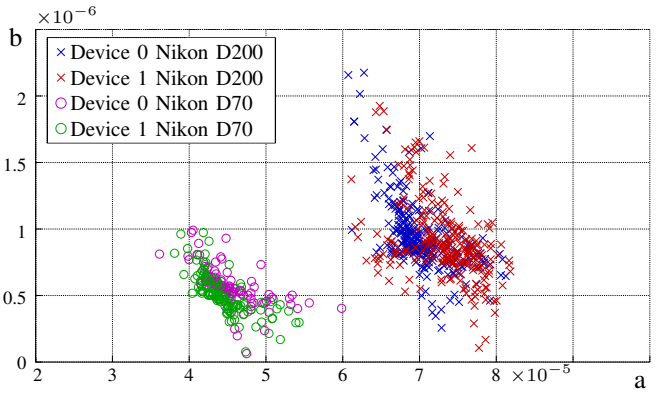

Fig. 3: Estimated camera parameters (a, b) of different devices per camera model with ISO 200 and different camera settings.

In fact, in the relation (4) and (6), the parameter a may not be equal to the analog gain g in practice due to the spatial variation in the pixel response, e.g. PRNU. However its effect is negligible in the heteroscedastic noise model. Moreover, this can be also justified due to the fact that the estimation methodology of the parameters (a, b) works on assumption that the pixels are independent and identically distributed in each homogeneous segment extracted by the segmentation (see Section III).

The heteroscedastic noise model (3) characterizes the response of a digital imaging sensor. This noise model accounts for the noises corrupting the raw image at the sensor output. Moreover, this noise model shows a linear relation between pixel's expectation and variance. An example is given in Fig. 1 which illustrates the heteroscedastic relation between pixels' expectation and variance for *Nikon D70* and *Nikon D200* from the Dresden image database [30]. For a fixed ISO sensitivity, the camera parameters (a, b) are discriminative for different camera models. The Fig. 1 and Fig. 2 illustrate the discriminability of parameters (a, b). However, the parameters

(a, b) can not separate different devices of the same model because of the same sensor characteristics, see Fig. 3. This paper proposes to exploit the camera parameters (a, b) for camera model identification.

III. Camera Parameter Estimation

details and edges) in the homogeneous regions. Therefore, the outliers need to be removed from homogeneous regions to achieve more accurate local estimates, leading to more accurate noise model parameters.

It is important to remind that the paper focuses on designing a GLRT with analytic performance. Therefore, the camera parameters (a, b) need to be estimated based on the Maximum Likelihood (ML) approach. The ML estimates of parameters (a, b) were first proposed in [28]. However, they can not be analytically given due to a difficulty of finding a solution of the first derivative of likelihood function. They are only numerically solved in the framework of maximization problem of likelihood function by using the Nelder-Mead optimization method [31]. Although this method estimates the parameters (a, b) with relative accuracy, it involves three main drawbacks. First, the convergence of the maximization process and the sensitivity of the solution to initial conditions have not been analyzed yet. Second, the Bayesian approach is used in [28] with a fixed uniform distribution which might be doubtful in practice. Finally, it is too difficult to provide statistical properties of the estimates. This leads to an impossibility of analytically establishing the statistical performance of the GLRT.

In regards to these drawbacks, this paper proposes an estimation of parameters (a, b) based on the WLS approach [32], [33]. As explained in [32], [33], when the weights are consistently estimated, the WLS estimates are asymptotically equivalent to the ML estimates in large samples. Accordingly, they can be used to design the GLRT.

This paper follows the segmentation method proposed in [28] (see more details in [28]). The image $\mathbf{Z}$ is first transformed into the wavelet domain and then segmented into K non-overlapping homogeneous segments, denoted S_k, of size n_k, $k \in \{1, \ldots, K\}$. In each segment S_k, pixels are supposedly independent and identically distributed. Let $\mathbf{z}_k^{\text{wapp}} = \{z_{k,i}^{\text{wapp}}\}_{i=1}^{n_k}$ and $\mathbf{z}_k^{\text{wdet}} = \{z_{k,i}^{\text{wdet}}\}_{i=1}^{n_k}$ be respectively the vector of wavelet approximation coefficients and wavelet detail coefficients representing the segment S_k. Because transformation is linear, the coefficients $z_{k,i}^{\text{wapp}}$ and $z_{k,i}^{\text{wdet}}$ also follow the Gaussian distribution

$$z_{k,i}^{\text{wapp}} \sim \mathcal{N}(\mu_k, \|\varphi\|_2^2\, \sigma_k^2) \tag{7}$$

$$z_{k,i}^{\text{wdet}} \sim \mathcal{N}(0, \sigma_k^2) \tag{8}$$

where $\sigma_k^2 = a\mu_k + b$ and φ is the 2-D normalized wavelet scaling function. Hence, the ML estimates of local mean μ_k and local variance $\hat{\nu}_k$ are given by

$$\hat{\mu}_k = \frac{1}{n_k} \sum_{i=1}^{n_k} z_{k,i}^{\text{wapp}} \tag{9}$$

$$\hat{\nu}_k = \frac{1}{n_k - 1} \sum_{i=1}^{n_k} (z_{k,i}^{\text{wdet}} - \overline{z}_k^{\text{wdet}})^2 \tag{10}$$

where $\overline{z}_k^{\text{wdet}} = \frac{1}{n_k} \sum_{i=1}^{n_k} z_{k,i}^{\text{wdet}}$. The estimate $\hat{\mu}_k$ is unbiased and follows the Gaussian distribution

$$\hat{\mu}_k \sim \mathcal{N}(\mu_k, c_k \sigma_k^2) \tag{11}$$

where $c_k = \frac{\|\varphi\|_2^2}{n_k}$ while the estimate $\hat{\nu}_k$ follows a scale chi-square distribution with $n_k - 1$ degrees of freedom. This distribution can also be accurately approximated as the Gaussian distribution for large n_k [34]:

$$\hat{\nu}_k \sim \mathcal{N}(\sigma_k^2,\, e_k \sigma_k^4) \tag{12}$$

where $e_k = \frac{2}{n_k}$. The Fig. 1 shows a scatter-plot of all the pairs $\{(\hat{\mu}_k, \hat{\nu}_k)\}$ extracted from a real natural raw image of *Nikon D70* and *Nikon D200* cameras.

The parameters (a, b) are estimated by considering all the pairs $\{(\hat{\mu}_k, \hat{\nu}_k)\}_{k=1}^{K}$ where the local variance $\hat{\nu}_k$ is treated as a heteroscedastic model of the local mean $\hat{\mu}_k$. This model is formulated as follows [33]

$$\hat{\nu}_k = a\hat{\mu}_k + b + s_k \epsilon_k \tag{13}$$

where ϵ_k are independent and identically distributed as standard Gaussian and s_k is a function of the local mean μ_k. A direct calculation shows that

$$\begin{aligned} s_k^2 &= \text{Var}\big[\hat{\nu}_k\big] - \text{Var}\big[a\hat{\mu}_k + b\big] \\ &= e_k \sigma_k^4 - a^2 c_k \sigma_k^2 \\ &= e_k (a\mu_k + b)^2 - a^2 c_k (a\mu_k + b). \end{aligned} \tag{14}$$

The heteroscedasticity in the model (13) is governed by different s_k. The WLS approach aims to minimize the weighted residuals and provide a fitted model. A popular strategy for estimating (a, b) is to first obtain estimates $\hat{s}_k^2$ of the residuals s_k^2 and then apply WLS approach using weights $\hat{w}_k = \frac{1}{\hat{s}_k^2}$. The residuals s_k^2 are estimated using the Ordinary Least Squares (OLS) estimates [35] $(\hat{a}_L, \hat{b}_L)$ which are given by :

$$\begin{pmatrix} \hat{a}_L \\ \hat{b}_L \end{pmatrix} = (\mathbf{H}^T \mathbf{H})^{-1} \mathbf{H}^T \mathbf{V} \tag{15}$$

where

$$\mathbf{H} = \begin{pmatrix} \hat{\mu}_1 & 1 \\ \vdots & \vdots \\ \hat{\mu}_K & 1 \end{pmatrix} \quad \mathbf{V} = \begin{pmatrix} \hat{\nu}_1 \\ \vdots \\ \hat{\nu}_K \end{pmatrix}.$$

Therefore, the consistent estimates $\hat{s}_k^2$ can be directly computed as

$$\hat{s}_k^2 = e_k (\hat{a}_L \hat{\mu}_k + \hat{b}_L)^2 - \hat{a}_L^2 c_k (\hat{a}_L \hat{\mu}_k + \hat{b}_L). \tag{16}$$

By using the estimated weights $\hat{w}_k = \frac{1}{\hat{s}_k^2}$, the WLS estimates are defined by

$$\begin{pmatrix} \hat{a} \\ \hat{b} \end{pmatrix} = (\mathbf{H}^T \mathbf{W} \mathbf{H})^{-1} \mathbf{H}^T \mathbf{W} \mathbf{V} \tag{17}$$

where $\mathbf{W} = \text{diag}(\hat{w}_1, \ldots, \hat{w}_K)$. The WLS estimates follow the asymptotic bivariate Gaussian distribution

$$\begin{pmatrix} \hat{a} \\ \hat{b} \end{pmatrix} \sim \mathcal{N}\left(\begin{pmatrix} a \\ b \end{pmatrix}, \mathbf{\Sigma}_{ab} \right) \tag{18}$$

where $\mathbf{\Sigma}_{ab}$ denotes the asymptotic covariance matrix of WLS estimates $(\hat{a}, \hat{b})$

$$\mathbf{\Sigma}_{ab} = \begin{pmatrix} \sigma_a^2 & \sigma_{ab} \\ \sigma_{ab} & \sigma_b^2 \end{pmatrix}.$$

Here, σ_a^2, σ_b^2, σ_{ab} denote respectively the variance of $\hat{a}$, the variance of $\hat{b}$ and the covariance between $\hat{a}$ and $\hat{b}$. The covariance matrix $\mathbf{\Sigma}_{ab}$ is defined in Appendix A.

IV. Optimal Detector for Camera Model Identification Problem

A. Hypothesis Testing Formulation

The paper aims to identify camera models based on the heteroscedastic noise model (3). The camera model identification problem is cast in the framework of hypothesis testing theory. Let analyze two camera models 0 and 1. Each camera model j, $j \in \{0, 1\}$ is characterized by two parameters (a_j, b_j) for a fixed ISO sensitivity. In a binary hypothesis testing, the inspected image $\mathbf{Z} = \{z_i\}_{i \in \mathcal{I}}$ is either acquired by camera model 0 or camera model 1. The goal of the test is to decide between two hypotheses defined by $\forall i \in \mathcal{I}$

$$\begin{cases} \mathcal{H}_0 = \Big\{ z_i \sim \mathcal{N}(\mu_i, a_0\mu_i + b_0) \Big\} \\ \mathcal{H}_1 = \Big\{ z_i \sim \mathcal{N}(\mu_i, a_1\mu_i + b_1), (a_1, b_1) \neq (a_0, b_0) \Big\}. \end{cases} \tag{19}$$

As previously explained, this paper focuses on guaranteeing a prescribed false-alarm probability. Hence, let

$$\mathcal{K}_{\alpha_0} = \Big\{ \delta : \sup_{\boldsymbol{\theta}} \mathbb{P}_{\mathcal{H}_0} \Big[\delta(\mathbf{Z}) = \mathcal{H}_1 \Big] \leq \alpha_0 \Big\}$$

be the class of tests with a false alarm probability upper-bounded by α_0. Here $\mathbb{P}_{\mathcal{H}_j}(E)$ stands for the probability of event E under hypothesis $\mathcal{H}_j$, $j \in \{0, 1\}$, and the supremum over $\boldsymbol{\theta}$ has to be understood as whatever model parameters might be. Among all the tests in the class $\mathcal{K}_{\alpha_0}$, it is aimed at finding a test δ which maximizes the power function, defined by the correct detection probability:

$$\beta_\delta = \mathbb{P}_{\mathcal{H}_1} \Big[\delta(\mathbf{Z}) = \mathcal{H}_1 \Big].$$

The problem (19) highlights three fundamental difficulties of the camera model identification. First, even when all model parameters (μ_i, a_j, b_j), $i \in \mathcal{I}$, $j \in \{0, 1\}$, are known, the most powerful test, namely the LRT, has never been studied in the literature.

The second difficulty concerns unknown image parameters μ_i in practice. A possible approach to deal with unknown parameters consists in eliminating them by using the invariance principle [25]. This approach has been discussed in [36], [37] and has achieved a good performance in some applications [38]. However, in the heteroscedastic noise model, the image parameter μ_i appears in both mathematical expectation and variance of the pixel z_i. The invariant approach may not be applied due to a difficulty of finding a group of transformation under which the problem remains invariant. Another approach is to design a GLRT by replacing the unknown parameters by ML estimates [39]. The main challenge of this approach is to provide accurate ML estimates with statistical properties in order to analytically establish the detection performance of the GLRT.

Finally, the two hypotheses $\mathcal{H}_0$ and $\mathcal{H}_1$ are composite because the camera parameters (a_0, b_0) and (a_1, b_1) are unknown in practice. For the sake of clarity, this paper assumes that the camera parameters (a_0, b_0) are known and it only solves the problem in which the alternative hypothesis $\mathcal{H}_1$ is composite, i.e. the camera parameters (a_1, b_1) are unknown. It can be noted that a test that maximizes the detection power whatever (a_1, b_1) might scarcely exist. The main goal of this paper is to study the LRT and to design the GLRT to address the second and third difficulties.

Moreover, it should be highlighted that the GLRT dealing with unknown image parameters when the camera parameters are known can be interpreted as a closed hypothesis testing where a given image is either acquired by camera model 0 or camera model 1. Meanwhile, the GLRT dealing with unknown camera parameters (a_1, b_1) becomes an open hypothesis testing in which whether a given image is acquired by camera model 0. The given image is allowed to be acquired by an unknown camera model. Therefore, two proposed tests can be straightforwardly applied, depending on the demanding context.

B. Likelihood Ratio Test for Two Simple Hypotheses

When all model parameters are known, in virtue of the Neyman-Pearson lemma [25, theorem 3.2.1], the most powerful test δ solving the problem (19) is the LRT given by the following decision rule

$$\delta(\mathbf{Z}) = \begin{cases} \mathcal{H}_0 & \text{if} \quad \Lambda(\mathbf{Z}) = \displaystyle\sum_{i \in \mathcal{I}} \Lambda(z_i) < \tau \\ \mathcal{H}_1 & \text{if} \quad \Lambda(\mathbf{Z}) = \displaystyle\sum_{i \in \mathcal{I}} \Lambda(z_i) \geq \tau \end{cases} \tag{20}$$

where the decision threshold τ is the solution of the equation

$$\mathbb{P}_{\mathcal{H}_0} \Big[\Lambda(\mathbf{Z}) \geq \tau \Big] = \alpha_0 \tag{21}$$

to ensure that the LRT is in the class $\mathcal{K}_{\alpha_0}$. The Likelihood Ratio (LR) of one observation z_i is defined by

$$\begin{aligned} \Lambda(z_i) &= \log \left(\frac{\sigma_{i,0}}{\sigma_{i,1}} \right) + \frac{\sigma_{i,1}^2 - \sigma_{i,0}^2}{2\sigma_{i,1}^2\sigma_{i,0}^2} \, (z_i - \mu_i)^2 \\ &= \frac{1}{2} h_1(\mu_i) + \frac{1}{2} h_2(\mu_i)(z_i - \mu_i)^2 \end{aligned} \tag{22}$$

where the variance $\sigma_{i,j}^2 = a_j\mu_i + b_j$ and two functions $h_1(x)$ and $h_2(x)$ are defined by

$$h_1(x) = \log \frac{a_0 x + b_0}{a_1 x + b_1} \tag{23}$$

$$h_2(x) = \frac{1}{a_0 x + b_0} - \frac{1}{a_1 x + b_1}. \tag{24}$$

In order to analytically establish the statistical performance of the LRT, it is necessary to characterize the statistical distribution of the LR $\Lambda(\mathbf{Z})$ under each hypothesis $\mathcal{H}_j$. From

$z_i \sim \mathcal{N}(\mu_i, \sigma_{i,j}^2)$, $j \in \{0,1\}$, the two first moments of $\Lambda(z_i)$ under hypothesis $\mathcal{H}_j$ are given by

$$\mathbb{E}_{\mathcal{H}_j}\Big[\Lambda(z_i)\Big] = \frac{1}{2}h_1(\mu_i) + \frac{1}{2}h_2(\mu_i)\sigma_{i,j}^2 \tag{25}$$

$$\mathrm{Var}_{\mathcal{H}_j}\Big[\Lambda(z_i)\Big] = \frac{1}{2}h_2^2(\mu_i)\sigma_{i,j}^4 \tag{26}$$

where $\mathbb{E}_{\mathcal{H}_j}[\cdot]$ and $\mathrm{Var}_{\mathcal{H}_j}[\cdot]$ denote respectively the mathematical expectation and variance under hypothesis $\mathcal{H}_j$. Because of a large number of pixels in any natural image, in virtue of the Lindeberg Central Limit Theorem (CLT) [25, theorem 11.2.5], the statistical distribution of the LR $\Lambda(\mathbf{Z})$ is given by

$$\Lambda(\mathbf{Z}) \xrightarrow{D} \mathcal{N}\Big(m_j, v_j\Big) \quad \text{under} \quad \mathcal{H}_j,\ j \in \{0,1\}, \tag{27}$$

where the notation $\xrightarrow{D}$ denotes the convergence in distribution and

$$m_j = \sum_{i=1}^{N}\left[\frac{1}{2}h_1(\mu_i) + \frac{1}{2}h_2(\mu_i)\sigma_{i,j}^2\right] \tag{28}$$

$$v_j = \sum_{i=1}^{N}\frac{1}{2}h_2^2(\mu_i)\sigma_{i,j}^4. \tag{29}$$

Since a natural raw image is heterogeneous, it is proposed to normalize the LR $\Lambda(\mathbf{Z})$ in order to set the decision threshold independently of the image content. The normalized LR is defined by

$$\Lambda^\star(\mathbf{Z}) = \frac{\Lambda(\mathbf{Z}) - m_0}{\sqrt{v_0}}. \tag{30}$$

Accordingly, the corresponding test $\delta^\star$ is rewritten as follows

$$\delta^\star(\mathbf{Z}) = \begin{cases}\mathcal{H}_0 & \text{if} \quad \Lambda^\star(\mathbf{Z}) < \tau^\star \\ \mathcal{H}_1 & \text{if} \quad \Lambda^\star(\mathbf{Z}) \geq \tau^\star\end{cases} \tag{31}$$

The fact of normalizing the LR $\Lambda(\mathbf{Z})$ allows the test $\delta^\star$ to be applicable to any natural raw image since the normalized LR $\Lambda^\star(\mathbf{Z})$ follows the standard Gaussian distribution under hypothesis $\mathcal{H}_0$. The decision threshold $\tau^\star$ and the power function $\beta_{\delta^\star}$ are given in two following theorems.

Theorem 1. *Assuming that all the model parameters (μ_i, a_j, b_j), $i \in \mathcal{I}$, $j \in \{0,1\}$ are exactly known, the decision threshold of the test $\delta^\star$ is given by*

$$\tau^\star = \Phi^{-1}(1-\alpha_0) \tag{32}$$

where $\Phi(\cdot)$ and $\Phi^{-1}(\cdot)$ denotes respectively the cumulative distribution function of the standard Gaussian random variable and its inverse.

Theorem 2. *The power function of the test $\delta^\star$ is given by*

$$\beta_{\delta^\star} = 1 - \Phi\left(\frac{m_0 - m_1 + \tau^\star\sqrt{v_0}}{\sqrt{v_1}}\right). \tag{33}$$

The detection power $\beta_{\delta^\star}$ serves as an upper-bound of any statistical test for the camera model identification problem. The test $\delta^\star$ allows to warrant a prescribed false alarm rate and maximizes the detection probability. Since its statistical performance is analytically established, it can provide an analytically predictable result for any false alarm probability α_0.

In fact, the LRT aims at finding a decision using the ratio between the Maximum Likelihood function of a given image under alternative hypothesis $\mathcal{H}_1$ characterized by the camera parameters (a_1, b_1) and its Maximum Likelihood function under null hypothesis $\mathcal{H}_0$ characterized by the camera parameters (a_0, b_0). If this ratio is smaller than a threshold, the null hypothesis $\mathcal{H}_0$ is accepted. Conversely, the alternative hypothesis $\mathcal{H}_1$ is accepted. Therefore, the smaller the distance between two points (a_0, b_0) and (a_1, b_1) is, the more difficult the camera model identification is.

V. Generalized Likelihood Ratio Test with Unknown Image Parameters

The GLRT designed in this section deals with the difficulty of unknown image parameters μ_i assuming that the camera parameters (a_0, b_0) and (a_1, b_1) are known, i.e. the inspected image $\mathbf{Z}$ is either acquired by camera model 0 or camera model 1.

It can be noted that the number of unknown image parameters μ_i grows with the number of pixels N. Therefore, a preprocessing stage consisting in segmenting the inspected image $\mathbf{Z}$ into K non-overlapping homogeneous segments S_k of size n_k is performed to reduce the number of unknown parameters. Using the ML estimates $\hat{\mu}_k$ defined in (9), the GLRT $\widehat{\delta}_1$ is designed as follows

$$\widehat{\delta}_1 = \begin{cases}\mathcal{H}_0 & \text{if} \quad \widehat{\Lambda}_1(\mathbf{Z}) = \displaystyle\sum_{k=1}^{K}\sum_{i=1}^{n_k}\widehat{\Lambda}_1(z_{k,i}^{\mathrm{wapp}}) < \widehat{\tau}_1 \\ \mathcal{H}_1 & \text{if} \quad \widehat{\Lambda}_1(\mathbf{Z}) = \displaystyle\sum_{k=1}^{K}\sum_{i=1}^{n_k}\widehat{\Lambda}_1(z_{k,i}^{\mathrm{wapp}}) \geq \widehat{\tau}_1\end{cases} \tag{34}$$

where, again to ensure $\widehat{\delta}_1$ to be in the class $\mathcal{K}_{\alpha_0}$, $\widehat{\tau}_1$ is the solution of the equation

$$\mathbb{P}_{\mathcal{H}_0}\Big[\widehat{\Lambda}_1(\mathbf{Z}) \geq \widehat{\tau}_1\Big] = \alpha_0 \tag{35}$$

and the Generalized Likelihood Ratio (GLR) $\widehat{\Lambda}_1(z_{k,i}^{\mathrm{wapp}})$ is given by

$$\widehat{\Lambda}_1(z_{k,i}^{\mathrm{wapp}}) = \frac{1}{2}h_1(\hat{\mu}_k) + \frac{1}{2}h_2(\hat{\mu}_k)\frac{(z_{k,i}^{\mathrm{wapp}} - \hat{\mu}_k)^2}{\|\varphi\|_2^2}. \tag{36}$$

By invoking again the Lindeberg CLT, the statistical distribution of the GLR $\widehat{\Lambda}_1(\mathbf{Z})$ under hypothesis $\mathcal{H}_j$, $j \in \{0,1\}$, is given by (see details in Appendix B)

$$\widehat{\Lambda}_1(\mathbf{Z}) \xrightarrow{D} \mathcal{N}\Big(m_j^{(1)}, v_j^{(1)}\Big) \tag{37}$$

where $m_j^{(1)}$ and $v_j^{(1)}$ are respectively the mathematical expectation and variance of the GLR $\widehat{\Lambda}_1(\mathbf{Z})$

$$m_j^{(1)} = \sum_{k=1}^{K}\frac{n_k}{2}\left[h_1(\mu_k) + h_2(\mu_k)\sigma_{k,j}^2\Big(1 + \frac{1}{n_k}\Big)\right] \tag{38}$$

$$v_j^{(1)} = \sum_{k=1}^{K}\frac{n_k}{4}\Bigg[(h_1'(\mu_k))^2 c_k\sigma_{k,j}^2 + 2h_2^2(\mu_k)\sigma_{k,j}^4\Big(1 + \frac{1}{n_k}\Big)^2 + 3(h_2'(\mu_k))^2 c_k\sigma_{k,j}^6\Big(1 + \frac{1}{n_k}\Big)^2\Bigg] \tag{39}$$

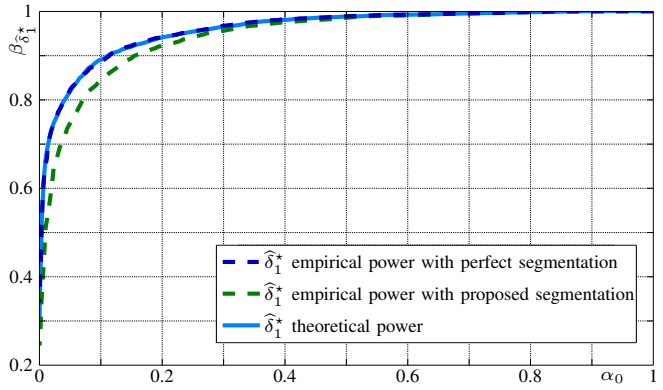

Fig. 4: The detection performance of the test $\widehat{\delta}_1^\star$ with 50 pixels selected randomly on simulated images.

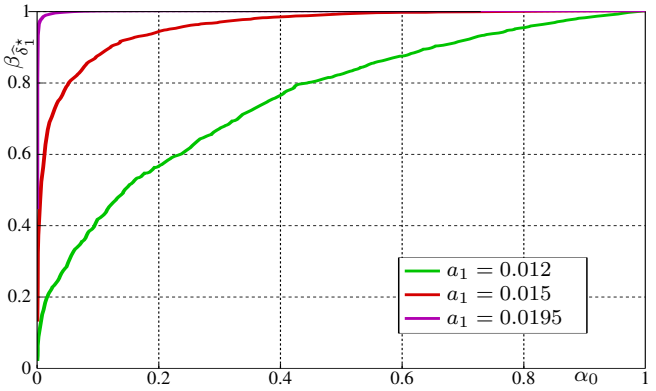

Fig. 5: The detection performance of the test $\widehat{\delta}_1^\star$ with 200 pixels selected randomly on simulated images for $a_0 = 0.0115$ and different parameters a_1.

where $\sigma_{k,j}^2 = a_j\mu_k + b_j$ and two derivatives $h_1'(x)$ and $h_2'(x)$ are defined in (101) and (102), respectively.

Similar to the LRT, the normalized GLR $\widehat{\Lambda}_1^\star(\mathbf{Z})$ is given by

$$\widehat{\Lambda}_1^\star(\mathbf{Z}) = \frac{\widehat{\Lambda}_1(\mathbf{Z}) - m_0^{(1)}}{\sqrt{v_0^{(1)}}}. \tag{40}$$

However, the expectation $m_0^{(1)}$ and the variance $v_0^{(1)}$ are not defined since the image parameters μ_k are unknown in practice. It is proposed to replace μ_k by $\hat{\mu}_k$ to obtain the estimates of $m_0^{(1)}$ and $v_0^{(1)}$, denoted $\hat{m}_0^{(1)}$ and $\hat{v}_0^{(1)}$ respectively

$$\widehat{\Lambda}_1^\star(\mathbf{Z}) = \frac{\widehat{\Lambda}_1(\mathbf{Z}) - \hat{m}_0^{(1)}}{\sqrt{\hat{v}_0^{(1)}}}. \tag{41}$$

The corresponding test $\widehat{\delta}_1^\star$ is rewritten as follows

$$\widehat{\delta}_1^\star(\mathbf{Z}) = \begin{cases} \mathcal{H}_0 & \text{if} \quad \widehat{\Lambda}_1^\star(\mathbf{Z}) < \widehat{\tau}_1^\star \\ \mathcal{H}_1 & \text{if} \quad \widehat{\Lambda}_1^\star(\mathbf{Z}) \geq \widehat{\tau}_1^\star \end{cases} \tag{42}$$

From the Slutsky's theorem [25, theorem 11.2.11], one obtains straightforwardly the decision threshold and the power function of the test $\widehat{\delta}_1^\star$

Theorem 3. *When the parameters (a_0, b_0) and (a_1, b_1) are known, the decision threshold of the test $\widehat{\delta}_1^\star$ is given by*

$$\widehat{\tau}_1^\star = \Phi^{-1}(1 - \alpha_0). \tag{43}$$

Theorem 4. *The power function of the test $\widehat{\delta}_1^\star$ is given by*

$$\beta_{\widehat{\delta}_1^\star} = 1 - \Phi\left(\frac{m_0^{(1)} - m_1^{(1)} + \widehat{\tau}_1^\star\sqrt{v_0^{(1)}}}{\sqrt{v_1^{(1)}}}\right). \tag{44}$$

VI. Generalized Likelihood Ratio Test with Unknown Image and Camera Parameters

This section designs a GLRT when the image parameters μ_i and the camera parameters (a_1, b_1) are unknown. The goal of this GLRT is to verify whether the inspected image is acquired by the camera model 0. The inspected image $\mathbf{Z}$ is allowed to be taken from an unknown camera model.

Using the ML estimates $\hat{\mu}_k$ and WLS estimates $(\hat{a}_1, \hat{b}_1)$ proposed in Section III, the GLRT $\widehat{\delta}_2$ is given as follows

$$\widehat{\delta}_2 = \begin{cases} \mathcal{H}_0 & \text{if} \quad \widehat{\Lambda}_2(\mathbf{Z}) = \displaystyle\sum_{k=1}^{K}\sum_{i=1}^{n_k} \widehat{\Lambda}_2(z_{k,i}^{\text{wapp}}) < \widehat{\tau}_2 \\ \mathcal{H}_1 & \text{if} \quad \widehat{\Lambda}_2(\mathbf{Z}) = \displaystyle\sum_{k=1}^{K}\sum_{i=1}^{n_k} \widehat{\Lambda}_2(z_{k,i}^{\text{wapp}}) \geq \widehat{\tau}_2 \end{cases} \tag{45}$$

where $\widehat{\tau}_2$ is the solution of the equation

$$\mathbb{P}_{\mathcal{H}_0}\left[\widehat{\Lambda}_2(\mathbf{Z}) \geq \widehat{\tau}_2\right] = \alpha_0 \tag{46}$$

and the GLR $\widehat{\Lambda}_2(z_{k,i}^{\text{wapp}})$ is defined by

$$\widehat{\Lambda}_2(z_{k,i}^{\text{wapp}}) = \log\frac{\hat{\sigma}_{k,0}}{\hat{\sigma}_{k,1}} + \frac{\hat{\sigma}_{k,1}^2 - \hat{\sigma}_{k,0}^2}{2\|\varphi\|_2^2\hat{\sigma}_{k,1}^2\hat{\sigma}_{k,0}^2}(z_{k,i}^{\text{wapp}} - \hat{\mu}_k)^2 \tag{47}$$

where $\hat{\sigma}_{k,0}^2 = a_0\hat{\mu}_k + b_0$ and $\hat{\sigma}_{k,1}^2 = \hat{a}_1\hat{\mu}_k + \hat{b}_1$. For brevity, let denote

$$\zeta_k = \log\frac{\hat{\sigma}_{k,0}^2}{\hat{\sigma}_{k,1}^2} \tag{48}$$

$$\gamma_k = \frac{1}{\hat{\sigma}_{k,0}^2} - \frac{1}{\hat{\sigma}_{k,1}^2} \tag{49}$$

The GLR $\widehat{\Lambda}_2(z_{k,i}^{\text{wapp}})$ (47) can be written as

$$\widehat{\Lambda}_2(z_{k,i}^{\text{wapp}}) = \frac{1}{2}\zeta_k + \frac{1}{2}\gamma_k\frac{(z_{k,i}^{\text{wapp}} - \hat{\mu}_k)^2}{\|\varphi\|_2^2}. \tag{50}$$

Firstly, it follows from the classical Delta method [25, theorem 11.2.14] that

$$\hat{\sigma}_{k,0}^2 \sim \mathcal{N}\left(\sigma_{k,0}^2, a_0^2c_k\sigma_{k,j}^2\right) \tag{51}$$

$$\log(\hat{\sigma}_{k,0}^2) \xrightarrow{D} \mathcal{N}\left(\log(\sigma_{k,0}^2), \frac{a_0^2c_k\sigma_{k,j}^2}{\sigma_{k,0}^4}\right) \tag{52}$$

$$\frac{1}{\hat{\sigma}_{k,0}^2} \xrightarrow{D} \mathcal{N}\left(\frac{1}{\sigma_{k,0}^2}, \frac{a_0^2c_k\sigma_{k,j}^2}{\sigma_{k,0}^8}\right). \tag{53}$$

Based on the definitions of expectation and variance, a short algebra shows that

$$\mathbb{E}_{\mathcal{H}_j}\left[\hat{\sigma}^2_{k,1}\right] = \sigma^2_{k,1} \tag{54}$$

$$\begin{aligned}\mathrm{Var}_{\mathcal{H}_j}\left[\hat{\sigma}^2_{k,1}\right] &= a^2 c_k \sigma^2_{k,j} + (\mu_k^2 + c_k\sigma^2_{k,j})\sigma^2_{a_1} \\ &\quad + 2\mu_k\sigma_{a_1 b_1} + \sigma^2_{b_1}.\end{aligned} \tag{55}$$

Moreover, from the Delta method [40], one obtains

$$\mathbb{E}_{\mathcal{H}_j}\left[\log(\hat{\sigma}^2_{k,1})\right] = \log(\sigma^2_{k,1}) \tag{56}$$

$$\mathrm{Var}_{\mathcal{H}_j}\left[\log(\hat{\sigma}^2_{k,1})\right] = \frac{\mathrm{Var}_{\boldsymbol{\theta}_{k,j}}\left[\hat{\sigma}^2_{k,1}\right]}{\sigma^4_{k,1}} \tag{57}$$

$$\mathbb{E}_{\mathcal{H}_j}\left[\frac{1}{\hat{\sigma}^2_{k,1}}\right] = \frac{1}{\sigma^2_{k,1}} \tag{58}$$

$$\mathrm{Var}_{\mathcal{H}_j}\left[\frac{1}{\hat{\sigma}^2_{k,1}}\right] = \frac{\mathrm{Var}_{\boldsymbol{\theta}_{k,j}}\left[\hat{\sigma}^2_{k,1}\right]}{\sigma^8_{k,1}}. \tag{59}$$

Therefore, the expectation and the variance of ζ_k under hypothesis $\mathcal{H}_j$ are defined by

$$\mathbb{E}_{\mathcal{H}_j}\left[\zeta_k\right] = \log\frac{\sigma^2_{k,0}}{\sigma^2_{k,1}} = h_1(\mu_k) \tag{60}$$

$$\mathrm{Var}_{\mathcal{H}_j}\left[\zeta_k\right] = \frac{a_0^2 c_k \sigma^2_{k,j}}{\sigma^4_{k,0}} + \frac{\mathrm{Var}_{\mathcal{H}_j}[\hat{\sigma}^2_{k,1}]}{\sigma^4_{k,1}}. \tag{61}$$

The expectation and the variance of γ_k under hypothesis $\mathcal{H}_j$ are defined by

$$\mathbb{E}_{\mathcal{H}_j}[\gamma_k] = \frac{1}{\sigma^2_{k,0}} - \frac{1}{\sigma^2_{k,1}} = h_2(\mu_k) \tag{62}$$

$$\mathrm{Var}_{\mathcal{H}_j}[\gamma_k] = \frac{a_0^2 c_k \sigma^2_{k,j}}{\sigma^8_{k,0}} + \frac{\mathrm{Var}_{\mathcal{H}_j}\left[\hat{\sigma}^2_{k,1}\right]}{\sigma^8_{k,1}}. \tag{63}$$

From (106), (107) and (60)-(63), one derives the two first moments of $\widehat{\Lambda}_3(z^{\mathrm{wapp}}_{k,i})$

$$\begin{aligned}\mathbb{E}_{\mathcal{H}_j}\left[\widehat{\Lambda}_2(z^{\mathrm{wapp}}_{k,i})\right] &= \frac{1}{2}h_1(\mu_k) \\ &\quad + \frac{1}{2}h_2(\mu_k)\sigma^2_{k,j}\left(1 + \frac{1}{n_{k,j}}\right)\end{aligned} \tag{64}$$

$$\begin{aligned}\mathrm{Var}_{\mathcal{H}_j}\left[\widehat{\Lambda}_2(z^{\mathrm{wapp}}_{k,i})\right] &= \frac{1}{4}\mathrm{Var}_{\mathcal{H}_j}\left[\zeta_k\right] \\ &\quad + \frac{1}{2}h_2^2(\mu_k)\sigma^4_{k,j}\left(1 + \frac{1}{n_k}\right)^2 \\ &\quad + \frac{3}{4}\sigma^4_{k,j}\left(1 + \frac{1}{n_k}\right)^2 \mathrm{Var}_{\mathcal{H}_j}\left[\gamma_k\right].\end{aligned} \tag{65}$$

Finally, it follows from the Lindeberg CLT that the statistical distribution of the GLR $\widehat{\Lambda}_2(\mathbf{Z})$ is given by

$$\widehat{\Lambda}_2(\mathbf{Z}) \xrightarrow{D} \mathcal{N}\left(m_j^{(2)}, v_j^{(2)}\right) \quad \text{under} \quad \mathcal{H}_j, j \in \{0,1\} \tag{66}$$

where $m_j^{(2)}$ and $v_j^{(2)}$ are respectively the asymptotic mathematical expectation and variance of the GLR $\widehat{\Lambda}_2(\mathbf{Z})$

$$m_j^{(2)} = \sum_{k=1}^{K} n_k \mathbb{E}_{\mathcal{H}_j}\left[\widehat{\Lambda}_2(z^{\mathrm{wapp}}_{k,i})\right] \tag{67}$$

$$v_j^{(2)} = \sum_{k=1}^{K} n_k \mathrm{Var}_{\mathcal{H}_j}\left[\widehat{\Lambda}_2(z^{\mathrm{wapp}}_{k,i})\right]. \tag{68}$$

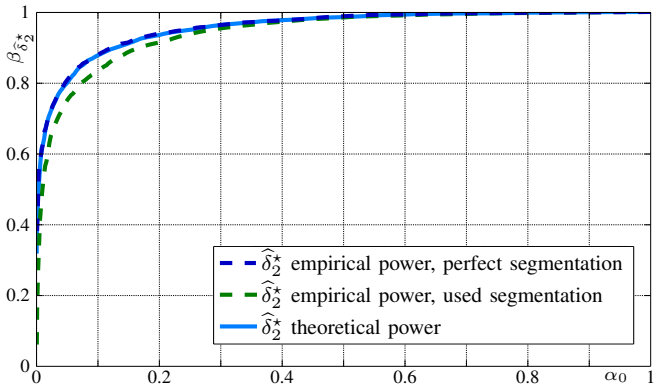

Fig. 6: The detection performance of the test $\widehat{\delta}^\star_2$ with 50 pixels selected randomly on simulated images.

Here, the expectation $m_j^{(2)}$ and the variance $v_j^{(2)}$ of the GLR $\widehat{\Lambda}_2(\mathbf{Z})$ will not be explicitly written due to the complicated form of $\mathbb{E}_{\mathcal{H}_j}\left[\widehat{\Lambda}_2(z^{\mathrm{wapp}}_{k,i})\right]$ and $\mathrm{Var}_{\mathcal{H}_j}\left[\widehat{\Lambda}_2(z^{\mathrm{wapp}}_{k,i})\right]$, see (64) and (65).

Similarly, the normalized GLR $\widehat{\Lambda}^\star_2(\mathbf{Z})$ is defined by

$$\widehat{\Lambda}^\star_2(\mathbf{Z}) = \frac{\widehat{\Lambda}_2(\mathbf{Z}) - \hat{m}_0^{(2)}}{\sqrt{\hat{v}_0^{(2)}}} \tag{69}$$

where $\hat{m}_0^{(2)}$ and $\hat{v}_0^{(2)}$ are the estimates of expectation $m_0^{(2)}$ and variance $v_0^{(2)}$ by replacing μ_k by $\hat{\mu}_k$ and (a_1, b_1) by $(\hat{a}_1, \hat{b}_1)$. The corresponding test $\widehat{\delta}^\star_2$ is rewritten as follows

$$\widehat{\delta}^\star_2(\mathbf{Z}) = \begin{cases}\mathcal{H}_0 & \text{if} \quad \widehat{\Lambda}^\star_2(\mathbf{Z}) < \widehat{\tau}^\star_2 \\ \mathcal{H}_1 & \text{if} \quad \widehat{\Lambda}^\star_2(\mathbf{Z}) \geq \widehat{\tau}^\star_2\end{cases} \tag{70}$$

From the Slutsky's theorem, the decision threshold and the power function of the test $\widehat{\delta}^\star_2$ are given in the following theorems.

Theorem 5. *When the camera parameters (a_0, b_0) are known and (a_1, b_1) are unknown, the decision threshold of the test $\widehat{\delta}^\star_2$ is given by*

$$\widehat{\tau}^\star_2 = \Phi^{-1}(1 - \alpha_0). \tag{71}$$

Theorem 6. *The power function of the test $\widehat{\delta}^\star_2$ is given by*

$$\beta_{\widehat{\delta}^\star_2} = 1 - \Phi\left(\frac{m_0^{(2)} - m_1^{(2)} + \widehat{\tau}^\star_2\sqrt{v_0^{(2)}}}{\sqrt{v_1^{(2)}}}\right). \tag{72}$$

VII. Numerical Experiments

A. Experimental Dataset

The test set includes cameras from Dresden image database [30], BOSS base [41] and our own database. Technical specifications of the cameras are shown in Table I. The test set covers different devices per camera model, different imaged scenes, different camera settings and different environmental conditions. The Dresden database [30] contains two devices per camera model. In case of the *Nikon D200* camera, two SLR-camera bodies were used with interchanging two different lenses for each acquired scene. Note that the BOSS base

TABLE I: Camera Model Used in Experiments (the symbol * indicates our own camera)

Camera Model		No. devices	Sensor size	Bit Depth	ISO Sensitivity	No. images
Nikon D70 [30], [41]	N70	3	23.7 × 15.6 mm CCD	12	200-400-800	1300
Nikon D90*	N90	2	23.6 × 15.8 mm CMOS	12	200-400-800	800
Nikon D200 [30]	N200	2	23.6 × 15.8 mm CCD	12	200	750
Canon 7D [41]	C7	1	22.3 × 14.9 mm CMOS	14	100	250
Canon 40D*	C40	2	22.2 × 14.8 mm CMOS	14	200-400-800	800
Canon 400D [41]	C400	1	22.2 × 14.8 mm CMOS	12	100-200-800	1300
Canon 450D*	C450	2	22.2 × 14.8 mm CMOS	14	100-400	800
Pentax K20D [41]	P	1	23.4 × 15.6 mm CMOS	12	100-200-400	1200

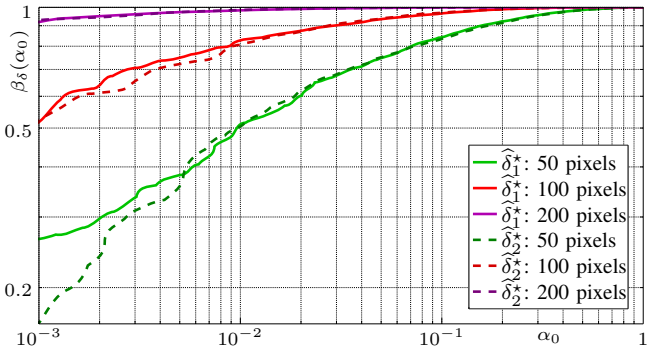

Fig. 7: The detection performance of the test $\widehat{\delta}_1^\star$ and $\widehat{\delta}_2^\star$ on simulated images for different numbers of pixels.

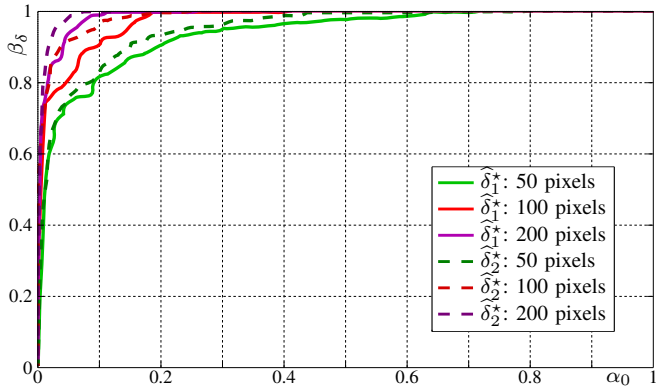

Fig. 8: The detection performance of the test $\widehat{\delta}_1^\star$ and $\widehat{\delta}_2^\star$ on the Dresden database for different numbers of pixels.

[41] also contains a *Nikon D70* camera device. Therefore, the test set finally contains 3 different devices of the *Nikon D70* camera model.

B. Simulated Images

The detection performance of the proposed tests $\widehat{\delta}_1^\star$ and $\widehat{\delta}_2^\star$ is first theoretically studied on a simulated data. The camera model 0 and 1 are respectively characterized by $a_0 = 0.0115$, $b_0 = 0.0002$, $a_1 = 0.0195$, $b_1 = 0.00025$. These parameters respectively correspond to *Nikon D70* and *Nikon D200* with ISO 200 estimated from the Dresden image database [30], see Fig. 1. Moreover, the values correspond to an 8-bit image in the normalized [0,1] scale. The camera parameters are used with 8-bit synthetic image of size 512×512 to generate

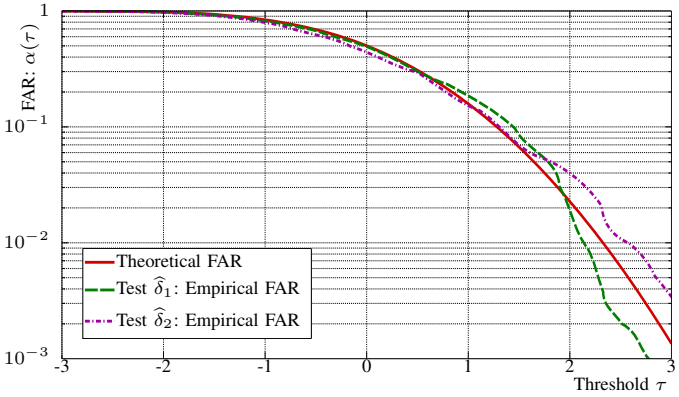

Fig. 9: Empirical false alarm probability from real images of Dresden database [30] plotted as a function of decision threshold.

randomly 5000 images for camera model 0 and 5000 images for camera model 1. The number of segments K is set to $K = 2^8$. The Fig. 4 and Fig. 6 illustrate respectively the detection performance of the tests $\widehat{\delta}_1^\star$ and $\widehat{\delta}_2^\star$ with 50 pixels selected randomly on the synthetic images. The segmentation method [28] used to obtain homogeneous segments is probably not perfect. Therefore, a slight error in the estimation of local means in each segment leads to a small loss of optimality. A perfect segmentation is not available in practice due to the difficulty of controlling noise in natural images and the influence of image content. The perfect segmentation can be performed in this simulation since the original synthetic image used to generate random images is available. The empirical power with perfect segmentation fits accurately to the theoretical power.

Additionally, it is desirable to observe the detection performance for different camera parameters. The test $\widehat{\delta}_1^\star$ is conducted by keeping the parameters (a_0, b_0) and setting a_1 to $\{0.0195, 0.015, 0.012\}$. As expected, the Fig. 5 shows that when the parameter a_1 tends to a_0, the power function of the test $\widehat{\delta}_1^\star$ declines and the Receiver Operating Characteristic (ROC) curves tends to $\beta_{\widehat{\delta}_1^\star} = \alpha_0$. In other words, the detection performance of the proposed tests depends on the discriminability of camera parameters (a, b).

The Fig. 7 illustrates in log-log scale the detection performance of the test $\widehat{\delta}_1^\star$ and $\widehat{\delta}_2^\star$ for $\{50, 100, 200\}$ pixels. A small loss of power is obviously revealed in case of 50 and 100 pixels between the tests $\widehat{\delta}_1^\star$ and $\widehat{\delta}_2^\star$ due to insufficient statistics.

TABLE II: Confusion matrix for ISO 100

		$\mathcal{H}_1$			
		C7	C400	C450	P
$\mathcal{H}_0$	C7	97.3	0	0	0
	C400	0	99.7	0	0
	C450	1.7	0	100	0
	P	0	0	0	99.8

TABLE III: Confusion matrix for ISO 200

		$\mathcal{H}_1$					
		N70	N90	N200	C40	C400	P
$\mathcal{H}_0$	N70	99.6	1.1	0.2	0	0	0
	N90	1.1	100	0	0	0	0
	N200	0	0	99.6	0	0	0
	C40	0	0	0	100	0	0
	C400	0	0	0	0	99.8	0
	P	0.7	0	0	0	0	99.8

TABLE IV: Confusion matrix for ISO 400

		$\mathcal{H}_1$			
		N70	N90	C40	P
$\mathcal{H}_0$	N70	100	0	0	0
	N90	0	100	0	0
	C40	0	0	100	0
	P	0	0	0	100

TABLE V: Confusion matrix for ISO 800

		$\mathcal{H}_1$			
		N70	N90	C40	C400
$\mathcal{H}_0$	N70	100	0	0	0
	N90	0	100	0	0
	C40	0	0	100	0
	C400	0	0	0	99.5

Both tests are identical with 200 pixels. Besides, the proposed tests are perfect with 500 pixels, i.e. no error of detection on 5000 simulated images from camera model 0 and 5000 simulated images from camera model 1.

Actually, the fact of selecting a number of pixels (e.g. 50, 100, 200 pixels) for the tests on the simulated data allows a better visibility since the empirical power function of the tests on 5000 simulated images is perfect (e.g. $\beta_\delta = 1$) with only 500 pixels. Moreover, on the contrary to other methods that exploit all the pixels, only a small number of pixels is used to achieve a perfect detection performance, which emphasizes the sharpness of the proposed tests.

C. Real Image Database

The experiments on simulated data give us an important insight : the proposed segmentation is probably not perfect, which leads to an error on pixels' expectation estimation. In practice, for real images, this task is more difficult since the presence of edges or details can cause poor estimates. Those outliers need to be removed because they can dramatically affect the detection performance of the proposed tests. This paper proposes to remove those outliers by the classical three-sigma rule [42]. Under normality, a pixel is considered as non-outlier if both following conditions are satisfied :

$$\begin{cases} \left|z_{k,i}^{\text{wapp}} - \hat{\mu}_k\right| & \leq 3\|\varphi\|_2\sqrt{\hat{a}\hat{\mu}_k + \hat{b}} \\ \left|z_{k,i}^{\text{wdet}}\right| & \leq 3\sqrt{\hat{a}\hat{\mu}_k + \hat{b}} \end{cases} \tag{73}$$

After outlier removal, all remaining pixels are used for the proposed tests.

To highlight the relevance of the proposed tests, two camera models from the same brand *Nikon D70* and *Nikon D200* of the Dresden image database [30] are chosen to conduct experiments since two camera models of the same brand are expected to exhibit similar characteristics. These cameras are set at the same ISO 200. Prior to our experiments, every raw image was converted to an uncompressed format using Dcraw (with parameters -D - T -4 -j -v) and was decomposed into 4 sub-images. Only the red color channel is used in experiments. The *Nikon D70* and *Nikon D200* cameras are respectively set at $\mathcal{H}_0$ and $\mathcal{H}_1$. The camera parameters are estimated on each image following the WLS approach. The parameters (a_0, b_0) and (a_1, b_1) are obtained by averaging the previously estimated values over 300 images. The Fig. 8 shows the detection performance of the test $\widehat{\delta}_1^\star$ and $\widehat{\delta}_2^\star$ for different numbers of pixels. Obviously, there is a small loss of power between the two power functions since the test $\widehat{\delta}_2^\star$ takes into account different estimates $(\hat{a}_1, \hat{b}_1)$ that are influenced by the image content. Nevertheless, two proposed tests are nearly perfect with 500 pixels, which is similar to the case of simulation. Besides, the Fig. 9 shows the comparison between the theoretical and empirical false alarm probability as a function of decision threshold $\alpha_0(\tau)$. While the test $\widehat{\delta}_1^\star$ shows its capacity of guaranteeing a prescribed false alarm rate, the test $\widehat{\delta}_2^\star$ fails in some cases (e.g. $-1 \leq \tau \leq 0$) due to the influence of image content and the presence of weak outliers that can not be detected by the above outlier removal process.

Experiments are then conducted on a large database to verify the efficiency of the proposed approach. Prior to the experiments, a training stage involves using 50 raw images per ISO sensitivity and per camera model to estimate the camera parameters (a_0, b_0). In the experiments, the test $\widehat{\delta}_2^\star$ is used to verify whether a given image is acquired by a certain camera model. The decision threshold $\hat{\tau}_2^\star$ is given by the Theorem 5 corresponding to the false alarm rate $\alpha_0 = 10^{-5}$. If the normalized GLR $\widehat{\Lambda}_2^\star(\mathbf{Z})$ is smaller than the decision threshold $\hat{\tau}_2^\star$, the hypothesis $\mathcal{H}_0$ is accepted. On the contrary, the hypothesis $\mathcal{H}_1$ is accepted. In the confusion matrix, each camera model is considered as hypothesis $\mathcal{H}_0$ (row) and all images that play a role as hypothesis $\mathcal{H}_1$ (column) are tested against $\mathcal{H}_0$. The values in the confusion matrix indicate the percentage of images that are detected taken from the camera model $\mathcal{H}_0$. It should be noted that the confusion matrix in this paper is not used in the same way as in the classification where the sum for each class yields 100%. This paper is based

TABLE VI: Confusion matrix by PRNU-based detector [18] for ISO 200

		$\mathcal{H}_1$					
		N70	N90	N200	C40	C400	P
$\mathcal{H}_0$	N70	97.9	0	0	0	0	0
	N90	0	85.5	0	0	0	0
	N200	0	0	100	0	0	0
	C40	0	0	0	100	0	0
	C400	0	0	0	0	99.8	0
	P	0	0	0	0	0	99.3

on a binary hypothesis testing in which the hypothesis $\mathcal{H}_0$ is always known in advance. The inspected image is brought into the testing between the hypothesis $\mathcal{H}_0$ against the others. Therefore, the sum of a class may not yield 100%. The results for each ISO 100, 200, 400, 800 are shown respectively in Table II, III, IV and V.

Potentially, there are many detectors in the literature for camera model identification, such as PRNU-based detector [22] and CFA-based detector [10], [11]. However, they are based on the fact that the fingerprint obtained from images in the TIFF or JPEG format contains traces of post-acquisition processes (e.g. demosaicing) that carry information about the camera model. This paper only focuses on raw images that have not gone through post-acquisition operations yet. Therefore, those detectors are not relevant to compare with the proposed detector. To the best of our knowledge, the proposed detector is the only one that focuses on raw images to identify camera models. The PRNU-based detector proposed in [17], [18] can deal with raw images but it was proposed for source device identification, which differs from camera model identification. Nevertheless, this detector is performed on the test set to compare with the proposed detector. Note that when the PRNU-based detector [22] for camera model identification is used for raw images that do not contain traces of post-acquisition processes, that detector reduces back to the one for source device identification. This paper uses 50 images per camera model to calculate a reference PRNU. Instead of the normalized correlation [17], the Peak to Correlation Energy (PCE) [18] is used as a test statistic for the decision problem. According to [18], the PCE is a more stable test statistic as it is independent of the image size and has other advantages such as its response to the presence of weak periodic signals. The decision threshold is given by $\tau = (\Phi^{-1}(\alpha_0))^2$ where $\alpha_0 = 10^{-5}$. If the test statistic PCE is greater than the decision threshold τ, the inspected image is detected taken from the camera $\mathcal{H}_0$. On the contrary, the image is detected taken from another camera. It should be noted that this detector does not depend on ISO sensitivity. However, to ensure that the experiments are conducted in the same scenario for the two detectors, only images with the same ISO from the same device are taken into account. Table VI shows the detection performance of the PRNU-based detector [18] for all images from the same device per camera model with ISO 200.

experiment is only performed on the cameras with at least three values of ISO sensitivity. The *Pentax K20D* camera is excluded from this experiment because the scatter-plots of $(\hat{a}, \hat{b})$ for ISO 100 and ISO 200 are very close for an unknown reason. The detection performance decreases significantly in case of the *Canon* brand when we mix all ISO sensitivity. In fact, the test $\widehat{\delta}_2^\star$ proposed here is rather sensible to the parameter a, see (19). We believe that the fact of adding a pedestal parameter causes an instability of the parameters (a, b). A significant difference between the estimate $\hat{a}$ and the true value a leads to a dramatic decline of detection performance.

VIII. Discussion

In the literature, most image forensic methods are based on imaging noise (e.g. PRNU) or post-acquisition operations (e.g. CFA interpolation) to identify a source device or a certain camera model. This paper relies on a different approach using the heteroscedastic noise model. In fact, this noise model accounts for all the noises corrupting the raw image at the sensor output. The parameters (a, b) characterizing the heteroscedastic noise model are considered as fingerprint to discriminate camera models. The main strength of the proposed approach is the designing of two GLRTs with analytic performance and the guaranteeing of a prescribed false alarm rate.

The main limitation is that the proposed approach mainly focuses on raw images that may not be available in practice. Since the proposed approach shows a nearly perfect detection performance, it is worth extending it to other image formats, e.g. TIFF and JPEG. The most challenging part when extending this work is the impact of post-acquisition enhancement and compression processes, see [4], [6] for a detailed study of image acquisition pipeline and statistical model of natural images after each process. Non-linear processes (e.g. gamma correction) modify the heteroscedastic noise model. Moreover, the spatial correlation caused by the demosaicing can lead to a difficulty of estimating accurately noise parameters. Another limitation is the dependence of the proposed approach on ISO sensitivity. However, this is not crucial because there are not many ISO sensitivity for a camera and only a small number of images are sufficient to estimate the parameters (a_0, b_0) (e.g. 50 images in this paper). Additionally, we can also exploit the relation between the camera parameters (a, b) and ISO sensitivity, as discussed in Section II-B, to avoid the dependence of the proposed detectors. However, the design of such detector lies out of the scope of the paper.

In terms of computational complexity, the algorithm depends on the number of segments K and the image size. In this paper, the number of segments K is set to the number of quantization levels, e.g. $K = 2^B$. Therefore, the algorithm is of the order of $O(N \cdot 2^B)$.

IX. Conclusion

This paper proposes a novel methodology for the camera model identification problem. The problem is cast in the framework of hypothesis testing theory. The approach is based on the heteroscedastic noise model. Two parameters (a, b) characterizing the heteroscedastic noise model are exploited as unique fingerprint for camera model identification. The

main strength of the proposed approach is the designing of two GLRTs with analytic performance that can be straightforwardly applied in the practical context. The main limitation is that this approach mainly focuses on raw images that may not be available in practice. Since the proposed approach shows a nearly perfect detection performance, it is worth extending it to other image formats, e.g. TIFF and JPEG. Moreover, future researches can also exploit this approach for the image forgery detection problem.

APPENDIX A
ASYMPTOTIC COVARIANCE MATRIX OF WLS ESTIMATES

Alternatively, the WLS estimates can be rewritten as

$$\hat{a} = \frac{\sum_{k=1}^{K} \hat{w}_k(\hat{\mu}_k - \hat{\overline{\mu}})\hat{\nu}_k}{\sum_{k=1}^{K} \hat{w}_k(\hat{\mu}_k - \hat{\overline{\mu}})^2} \tag{74}$$

$$\hat{b} = \hat{\overline{\nu}} - \hat{a}\hat{\overline{\mu}}. \tag{75}$$

where

$$\hat{\overline{\mu}} = \frac{\sum_{k=1}^{K} \hat{w}_k\hat{\mu}_k}{\sum_{k=1}^{K} \hat{w}_k} \tag{76}$$

$$\hat{\overline{\nu}} = \frac{\sum_{k=1}^{K} \hat{w}_k\hat{\nu}_k}{\sum_{k=1}^{K} \hat{w}_k}. \tag{77}$$

For brevity, let denote

$$U_1 = \sum_{k=1}^{K} \hat{w}_k(\hat{\mu}_k - \hat{\overline{\mu}})\hat{\nu}_k \quad \text{and} \quad U_2 = \sum_{k=1}^{K} \hat{w}_k(\hat{\mu}_k - \hat{\overline{\mu}})^2 \tag{78}$$

such that $\hat{a} = U_1/U_2$.

A. Statistical Properties of U_1 and U_2

It can be noted that $\hat{\mu}_k$ and $\hat{\nu}_k$ are mutually independent due to the orthogonality of the wavelets [28]. Moreover, the pair $(\hat{\mu}_i, \hat{\nu}_i)$ and $(\hat{\mu}_j, \hat{\nu}_j)$ are also mutually independent because the corresponding segment S_i and S_j are non-overlapping.

Because $(\hat{a}_L, \hat{b}_L)$ are the consistent estimates of (a, b), it follows from the Continuous Mapping Theorem [25, theorem 11.2.13] that

$$\hat{s}_k^2 \xrightarrow{P} s_k^2 \tag{79}$$

$$\hat{w}_k \xrightarrow{P} w_k \tag{80}$$

where the notation $\xrightarrow{P}$ denotes the convergence in probability. It follows from the Slutsky's Theorem [25, theorem 11.2.11] that

$$\hat{\overline{\mu}} \xrightarrow{D} \mathcal{N}\left(\overline{\mu},\ \frac{\sum_{k=1}^{K} w_k^2 c_k \sigma_k^2}{\left(\sum_{k=1}^{K} w_k\right)^2}\right) \tag{81}$$

$$\hat{\overline{\nu}} \xrightarrow{D} \mathcal{N}\left(\overline{\nu},\ \frac{\sum_{k=1}^{K} w_k^2 e_k \sigma_k^4}{\left(\sum_{k=1}^{K} w_k\right)^2}\right) \tag{82}$$

where

$$\overline{\mu} = \frac{\sum_{k=1}^{K} w_k\mu_k}{\sum_{k=1}^{K} w_k} \tag{83}$$

$$\overline{\nu} = \frac{\sum_{k=1}^{K} w_k\sigma_k^2}{\sum_{k=1}^{K} w_k} = a\overline{\mu} + b. \tag{84}$$

Based on the linearity property of the Gaussian distribution, it is easily shown that

$$\hat{\mu}_k - \hat{\overline{\mu}} \sim \mathcal{N}\Big(\mu_k - \overline{\mu},\ c_k\sigma_k^2 + \mathrm{Var}[\hat{\overline{\mu}}]\Big). \tag{85}$$

Combining (12) and (85), a direct calculation yields to

$$\mathbb{E}\Big[(\hat{\mu}_k - \hat{\overline{\mu}})\hat{\nu}_k\Big] = (\mu_k - \overline{\mu})\sigma_k^2 \tag{86}$$

$$\mathrm{Var}\Big[(\hat{\mu}_k - \hat{\overline{\mu}})\hat{\nu}_k\Big] = \sigma_k^4\Big[e_k(\mu_k - \overline{\mu})^2 + c_k\sigma_k^2\mathrm{Var}\big[\hat{\overline{\mu}}\big]\Big] + o(n_k^{-2}). \tag{87}$$

where the notation $x = o(y)$, with $y > 0$, means that $\frac{x}{y}$ tends to 0 as y tends to 0. Hence, the expectation and variance of U_1 are defined by

$$\mathbb{E}\big[U_1\big] = \sum_{k=1}^{K} w_k(\mu_k - \overline{\mu})\sigma_k^2 \tag{88}$$

$$\mathrm{Var}\big[U_1\big] = \sum_{k=1}^{K} w_k^2\sigma_k^4\Big[e_k(\mu_k - \overline{\mu})^2 + c_k\sigma_k^2 + \mathrm{Var}\big[\hat{\overline{\mu}}\big]\Big]. \tag{89}$$

From (85), based on the definitions of the mathematical expectation and the variance, one obtains

$$\mathbb{E}\Big[(\hat{\mu}_k - \hat{\overline{\mu}})^2\Big] = (\mu_k - \overline{\mu})^2 + c_k\sigma_k^2 + \mathrm{Var}\big[\hat{\overline{\mu}}\big] \tag{90}$$

$$\mathrm{Var}\Big[(\hat{\mu}_k - \hat{\overline{\mu}})^2\Big] = 4(\mu_k - \overline{\mu})^2\Big[c_k\sigma_k^2 + \mathrm{Var}\big[\hat{\overline{\mu}}\big]\Big] + o(n_k^{-2}). \tag{91}$$

Hence, the expectation and variance of U_2 are defined by

$$\mathbb{E}\big[U_2\big] = \sum_{k=1}^{K} w_k\Big[(\mu_k - \overline{\mu})^2 + c_k\sigma_k^2 + \mathrm{Var}\big[\hat{\overline{\mu}}\big]\Big] \tag{92}$$

$$\mathrm{Var}\big[U_2\big] = \sum_{k=1}^{K} 4w_k^2(\mu_k - \overline{\mu})^2\Big[c_k\sigma_k^2 + \mathrm{Var}\big[\hat{\overline{\mu}}\big]\Big]. \tag{93}$$

Based on the definition of the covariance, a direct calculation yields to

$$\begin{aligned}
&\mathrm{Cov}\Big[(\hat{\mu}_k - \hat{\overline{\mu}})\hat{\nu}_k, (\hat{\mu}_k - \hat{\overline{\mu}})^2\Big] \\
&= \mathbb{E}\Big[(\hat{\mu}_k - \hat{\overline{\mu}})^3\hat{\nu}_k\Big] - \mathbb{E}\Big[(\hat{\mu}_k - \hat{\overline{\mu}})\hat{\nu}_k\Big]\mathbb{E}\Big[(\hat{\mu}_k - \hat{\overline{\mu}})^2\Big] \\
&= \sigma_k^2\mathbb{E}\Big[(\hat{\mu}_k - \hat{\overline{\mu}})^3\Big] - \sigma_k^2\mathbb{E}\Big[(\hat{\mu}_k - \hat{\overline{\mu}})\Big]\mathbb{E}\Big[(\hat{\mu}_k - \hat{\overline{\mu}})^2\Big] \\
&= 2\sigma_k^2(\mu_k - \overline{\mu})\Big(c_k\sigma_k^2 + \mathrm{Var}\big[\hat{\overline{\mu}}\big]\Big).
\end{aligned} \tag{94}$$

Hence, the covariance between U_1 and U_2 is defined by

$$\begin{aligned}
\mathrm{Cov}\big[U_1, U_2\big] &= \sum_{k=1}^{K} w_k^2\mathrm{Cov}\Big[(\hat{\mu}_k - \hat{\overline{\mu}})\hat{\nu}_k, (\hat{\mu}_k - \hat{\overline{\mu}})^2\Big] \\
&= \sum_{k=1}^{K} 2w_k^2\sigma_k^2(\mu_k - \overline{\mu})\Big(c_k\sigma_k^2 + \mathrm{Var}\big[\hat{\overline{\mu}}\big]\Big).
\end{aligned} \tag{95}$$

B. Covariance Matrix Calculation

Therefore, from the classical Delta method [40] one can derive the variance σ_a^2

$$\begin{aligned}\sigma_a^2 &= \mathrm{Var}\Big[\frac{U_1}{U_2}\Big] \\ &= \frac{\mathrm{Var}\big[U_1\big]}{\mathbb{E}^2\big[U_2\big]} - \frac{2\mathbb{E}\big[U_1\big]}{\mathbb{E}^3\big[U_2\big]}\mathrm{Cov}\big[U_1,U_2\big] \\ &\quad + \frac{\mathbb{E}^2\big[U_1\big]}{\mathbb{E}^4\big[U_2\big]}\mathrm{Var}\big[U_2\big] + o\Big(\Big(\sum_{k=1}^{K} n_k^2\Big)^{-2}\Big) \end{aligned} \tag{96}$$

Additionally, the variance σ_b^2 and the covariance σ_{ab} are defined by

$$\begin{aligned}\sigma_b^2 &= \mathrm{Var}\big[\hat{\overline{\nu}} - \hat{a}\hat{\overline{\mu}}\big] \\ &= \mathrm{Var}\big[\hat{\overline{\nu}}\big] + a^2\mathrm{Var}\big[\hat{\overline{\mu}}\big] + \overline{\mu}^2\sigma_a^2 \\ &\quad + \sigma_a^2\mathrm{Var}\big[\hat{\overline{\mu}}\big] \end{aligned} \tag{97}$$

$$\sigma_{ab} = \mathrm{Cov}\big[\hat{a}, \hat{\overline{\nu}} - \hat{a}\hat{\overline{\mu}}\big] = -\overline{\mu}\sigma_a^2. \tag{98}$$

APPENDIX B
STATISTICAL DISTRIBUTION OF THE GLR $\widehat{\Lambda}_1(\mathbf{Z})$

For brevity, let denote

$$\rho_{k,i} = \frac{(z_{k,i}^{\mathrm{wapp}} - \hat{\mu}_k)^2}{\|\varphi\|_2^2} \tag{99}$$

such that

$$\widehat{\Lambda}_1(z_{k,i}^{\mathrm{wapp}}) = \frac{1}{2}h_1(\hat{\mu}_k) + \frac{1}{2}h_2(\hat{\mu}_k)\rho_{k,i}. \tag{100}$$

It can be noted that two functions h_1 and h_2 are continuous and differentiable on $\mathbb{R}^+$. Their first derivative can be expressed as

$$h_1'(x) = \frac{a_0b_1 - a_1b_0}{(a_0x+b_0)(a_1x+b_1)} \tag{101}$$

$$h_2'(x) = \frac{a_1}{(a_1x+b_1)^2} - \frac{a_0}{(a_0x+b_0)^2}. \tag{102}$$

These derivatives are equal to zero if and only if two cameras 0 and 1 are identical, i.e. $(a_0, b_0) = (a_1, b_1)$. For obvious reasons, this case is not considered in the present paper. Using the Delta method [25, theorem 11.2.14], it follows from (11) that

$$h_1(\hat{\mu}_k) \xrightarrow{D} \mathcal{N}\Big(h_1(\mu_k), (h_1'(\mu_k))^2c_k\sigma_{k,j}^2\Big) \tag{103}$$

$$h_2(\hat{\mu}_k) \xrightarrow{D} \mathcal{N}\Big(h_2(\mu_k), (h_2'(\mu_k))^2c_k\sigma_{k,j}^2\Big). \tag{104}$$

From (7) and (11), one obtains

$$z_{k,i}^{\mathrm{wapp}} - \hat{\mu}_k \sim \mathcal{N}\Big(0, \|\varphi\|_2^2\sigma_{k,j}^2\Big(1+\frac{1}{n_k}\Big)\Big) \tag{105}$$

Therefore, the mathematical expectation and variance of $\rho_{k,i}$ are given by

$$\mathbb{E}_{\mathcal{H}_j}\big[\rho_{k,i}\big] = \sigma_{k,j}^2\Big(1+\frac{1}{n_k}\Big) \tag{106}$$

$$\mathrm{Var}_{\mathcal{H}_j}\big[\rho_{k,i}\big] = 2\sigma_{k,j}^4\Big(1+\frac{1}{n_k}\Big)^2. \tag{107}$$

Consequently, the two first moments of $\widehat{\Lambda}_1(z_{k,i}^{\mathrm{wapp}})$ under hypothesis $\mathcal{H}_j$ are given by

$$\begin{aligned}\mathbb{E}_{\mathcal{H}_j}\Big[\widehat{\Lambda}_1(z_{k,i}^{\mathrm{wapp}})\Big] &= \frac{1}{2}h_1(\mu_k) \\ &\quad + \frac{1}{2}h_2(\mu_k)\sigma_{k,j}^2\Big(1+\frac{1}{n_k}\Big) \end{aligned} \tag{108}$$

$$\begin{aligned}\mathrm{Var}_{\mathcal{H}_j}\Big[\widehat{\Lambda}_1(z_{k,i}^{\mathrm{wapp}})\Big] &= \frac{1}{4}(h_1'(\mu_k))^2c_k\sigma_{k,j}^2 \\ &\quad + \frac{1}{2}h_2^2(\mu_k)\sigma_{k,j}^4\Big(1+\frac{1}{n_k}\Big)^2 \\ &\quad + \frac{3}{4}(h_2'(\mu_k))^2c_k\sigma_{k,j}^6\Big(1+\frac{1}{n_k}\Big)^2. \end{aligned} \tag{109}$$

In virtue of the Lindeberg CLT, it follows that under hypothesis $\mathcal{H}_j$: $\widehat{\Lambda}_1(\mathbf{Z}) \xrightarrow{D} \mathcal{N}\Big(m_j^{(1)}, v_j^{(1)}\Big)$ where

$$m_j^{(1)} = \sum_{k=1}^{K}\frac{n_k}{2}\Big[h_1(\mu_k) + h_2(\mu_k)\sigma_{k,j}^2\Big(1+\frac{1}{n_k}\Big)\Big] \tag{110}$$

$$\begin{aligned}v_j^{(1)} = \sum_{k=1}^{K}\frac{n_k}{4}\Big[&(h_1'(\mu_k))^2c_k\sigma_{k,j}^2 + 2h_2^2(\mu_k)\sigma_{k,j}^4\Big(1+\frac{1}{n_k}\Big)^2 \\ &+ 3(h_2'(\mu_k))^2c_k\sigma_{k,j}^6\Big(1+\frac{1}{n_k}\Big)^2\Big]. \end{aligned} \tag{111}$$

REFERENCES

[1] T. V. Lanh, K.-S. Chong, S. Emmanuel, and M. Kankanhalli, "A survey on digital camera image forensic methods," in *Multimedia and Expo, 2007 IEEE International Conference on*, 2007, pp. 16 – 19.

[2] T.-T. Ng, S.-F. Chang, C.-Y. Lin, and Q. Sun, "Passive-blind image forensics," in *In Multimedia Security Technologies for Digital Rights*, 2006.

[3] H. Farid, "A survey of image forgery detection," *IEEE Signal Processing Magazine*, vol. 2, no. 26, pp. 16 – 25, 2009.

[4] R. Ramanath, W. E. Snyder, Y. Yoo, and M. S. Drew, "Color image processing pipeline," *Signal Processing Magazine, IEEE*, vol. 22, no. 1, pp. 34 – 43, Jan. 2005.

[5] J. Nakamura, *Image Sensors and Signal Processing for Digital Still Cameras*. CRC Press, 2005.

[6] T. H. Thai, R. Cogranne, and F. Retraint, "Statistical Model of Natural Images," in *ICIP 2012, International Conference on Image Processing*, Sep. 2012, pp. 2525 – 2528.

[7] K. S. Choi, E. Y. Lam, and K. Wong, "Source camera identification using footprints from lens aberration," in *Proc. of the SPIE*, vol. 6069, Feb. 2006, pp. 172 – 179.

[8] M. Kharrazi, H. T. Sencar, and N. Memon, "Blind source camera identification," in *Image Processing International Conference on*, vol. 1, Oct. 2004, pp. 709 – 712.

[9] S. Bayram, H. Sencar, N. Memon, and I. Avcibas, "Source camera identification based on cfa interpolation," in *Image Processing, IEEE International Conference on*, vol. 3, Sept. 2005, pp. 69 – 72.

[10] A. Swaminathan, M. Wu, and K. J. R. Liu, "Nonintrusive component forensics of visual sensors using output images," *Information Forensics and Security, IEEE Transactions on*, vol. 2, no. 1, pp. 91 – 106, Mar. 2007.

[11] ——, "Digital image forensics via intrinsic fingerprints," *Information Forensics and Security, IEEE Transactions on*, vol. 3, no. 1, pp. 101 – 117, Mar. 2008.

[12] H. Cao and A. C. Kot, "Accurate detection of demosaicing regularity for digital image forensics," *Information Forensics and Security, IEEE Transactions on*, vol. 4, no. 4, pp. 899 – 910, Dec. 2009.

[13] K. S. Choi, E. Lam, and K. Wong, "Source camera identification by JPEG compression statistics for image forensics," in *TENCON 2006. 2006 IEEE Region 10 Conference*, Nov. 2006, pp. 1 – 4.

[14] Z. Deng, A. Gijsenij, and J. Zhang, "Source camera identification using auto-white balance approximation," in *Computer Vision (ICCV), 2011 IEEE International Conference on*, Nov. 2011, pp. 57 – 64.

[15] C. Scott, "Performance measures for Neyman-Pearson classification," *Information Theory, IEEE Transactions on*, vol. 53, no. 8, pp. 2852 –2863, Aug. 2007.

[16] J. Lukas, J. Fridrich, and M. Goljan, "Digital camera identification from sensor pattern noise," *Information Forensics and Security, IEEE Transactions on*, vol. 1, no. 2, pp. 205 – 214, Jun. 2006.

[17] M. Chen, J. Fridrich, M. Goljan, and J. Lukas, "Determining image origin and integrity using sensor noise," *Information Forensics and Security, IEEE Transactions on*, vol. 3, no. 1, pp. 74 – 90, Mar. 2008.

[18] M. Goljan, J. Fridrich, and T. Filler, "Large scale test of sensor fingerprint camera identification," in *Proc. SPIE, Electronic Imaging, Security and Forensics of Multimedia Contents XI*, vol. 7254, Jan. 2009, pp. 18 – 22.

[19] C.-T. Li, "Source camera identification using enhanced sensor pattern noise," *Information Forensics and Security, IEEE Transactions on*, vol. 5, no. 2, pp. 280 – 287, Jun. 2010.

[20] X. Kang, Y. Li, Z. Qu, and J. Huang, "Enhancing source camera identification performance with a camera reference phase sensor pattern noise," *Information Forensics and Security, IEEE Transactions on*, vol. 7, no. 2, pp. 393 – 402, Apr. 2012.

[21] C.-T. Li and Y. Li, "Color-decoupled photo response non-uniformity for digital image forensics," *Circuits and Systems for Video Technology, IEEE Transactions on*, vol. 22, no. 2, pp. 260 – 271, Feb. 2012.

[22] T. Filler, J. Fridrich, and M. Goljan, "Using sensor pattern noise for camera model identification," in *Image Processing, 15th IEEE International Conference on*, Oct. 2008, pp. 1296 – 1299.

[23] K. Kurosawa, K. Kuroki, and N. Saitoh, "CCD fingerprint method-identification of a video camera from videotaped images," in *Image Processing, International Conference on*, vol. 3, 1999, pp. 537 – 540.

[24] T. Gloe, M. Kirchner, A. Winkler, and R. Böhme, "Can we trust digital image forensics?" in *International Conference on Multimedia*, 2007, pp. 78 – 86.

[25] E. L. Lehmann and J. P. Romano, *Testing Statistical Hypotheses*, 3rd ed. Newyork: Springer, 2005.

[26] T. H. Thai, R. Cogranne, and F. Retraint, "Camera model identification based on hypothesis testing theory," in *Signal Processing Conference (EUSIPCO), 2012 Proceedings of the 20th European*, Aug. 2012, pp. 1747 – 1751.

[27] A. Foi, "Clipped noisy images : Heteroskedastic modeling and practical denoising," *Elsevier Signal Processing*, vol. 89, no. 12, pp. 2609 – 2629, Dec. 2009.

[28] A. Foi, M. Trimeche, V. Katkovnik, and K. Egiazarian, "Practical poissonian-gaussian noise modeling and fitting for single-image raw-data," *IEEE Trans. Image Process.*, vol. 17, no. 10, pp. 1737 – 1754, Oct. 2008.

[29] G. E. Healey and R. Kondepudy, "Radiometric ccd camera calibration and noise estimation," *IEEE Trans. Pattern Anal. Mach. Intell.*, vol. 16, pp. 267 – 276, Mar. 1994.

[30] T. Gloe and R. Bohme, "The 'dresden image database' for benchmarking digital image forensics," *Proc. ACM SAC*, vol. 2, pp. 1585– 1591, 2010.

[31] J. Nelder and R. Mead, "A simplex method for function minimization," *The Computer Journal*, vol. 7, pp. 308 – 313, 1965.

[32] J. Shao, "Asymptotic distribution of the weighted least squares estimator," *Ann. Inst. Statist Math.*, vol. 41, no. 2, pp. 365 – 382, 1989.

[33] R. Carroll, "Adapting for heteroscedasticity in linear models," *The Annals of Statistics*, vol. 10, no. 4, pp. 1224 – 1233, 1982.

[34] N. L. Johnson, S. Kotz, and N. Balakrishnan, *Continuous univariate distributions*, 2nd ed. Wiley, 1994.

[35] C. Rao and H. Toutenburg, *Linear models : Least Squares and Alternatives*, 2nd ed. Springer, 1999.

[36] M. Fouladirad and I. Nikiforov, "Optimal statistical fault detection with nuisance parameters," *Automatica*, vol. 41, pp. 1157 – 1171, 2005.

[37] L. Scharf and B. Friedlander, "Matched subspace detectors," *IEEE Trans. Signal Process.*, vol. 42, no. 8, pp. 2146 – 2157, 1994.

[38] L. Fillatre, I. Nikiforov, and F. Retraint, "Epsilon-optimal non-bayesian anomaly detection for parametric tomography," *IEEE Trans. Image Process.*, vol. 17, no. 11, pp. 1985 – 1999, 2008.

[39] D. Birkes, "Generalized likelihood ratio tests and uniformly most powerful tests," *The American Statistician*, vol. 44, no. 2, pp. 163 – 166, 1990.

[40] A. Stuart and J. Ord, *Kendall's Advanced Theory of Statistics*, 6th ed. Arnold, 1994, vol. 1.

[41] P. Bas, T. Filler, and T. Pevný, "Break our steganographic system — the ins and outs of organizing boss," in *Information Hiding, 13th International Workshop*, T. Filler, Ed., 2011.

[42] F. R. Hampel, "The influence curve and its role in robust estimation," *Journal of the American Statistical Association*, no. 69, pp. 382 – 393, 1974.